CURRENT-INDUCED LOADS ON MARINE STRUCTURES DUE TO VORTEX SHEDDING

OWEN M. GRIFFIN, Marine Technology Division, Naval Research Laboratory, Washington, DC 20375

ABSTRACT

This paper discusses available data for vortex-induced lift, drag, and displacement amplitude from numerous experiments which have been conducted over the past several years. It is clear from the results that there is a limiting amplitude of oscillation (± 1 or more diameters) as the transverse exciting force (and force coefficient C_{LE}) first increases from zero to a maximum ($C_{LE} = 0.5$ to 0.6) and then decreases again to zero as the limiting amplitude of displacement is approached. The mean in-line drag force also is increased as a result of the vibrations. Recent measurements of the hydrodynamic drag on freely-vibrating cylinders have shown that the drag coefficient is amplified by as much as 250 percent in water at large vibration amplitudes near the limiting value. For both the lift and drag measurements the Reynolds numbers were in the range $Re = 10^3$ to 10^4 and slightly higher. Thus the results are suitable for many practical applications for structures both in air and in water.

INTRODUCTION

A common mechanism for resonant, flow-excited oscillations is the organized and periodic shedding of vortices as the flow separates alternatively from opposite sides of a long, bluff body. If the structure is flexible and lightly damped internally, then resonant oscillations can be excited normal or parallel to the incident flow direction. For the more common cross flow oscillations, the body and the wake usually oscillate in unison at a frequency near one of the characteristic frequencies of the structure. This phenomenon is known as "lock-on" or "wake capture."

The vortex-excited oscillations of marine cables, commonly termed *strumming*, result in early fatigue, increased steady and unsteady hydrodynamic forces, and amplified acoustic flow noise. They sometimes lead to structural damage and to failure. Flow-excited oscillations very

often are a critical factor in the design of underwater cable arrays, tension leg platform tethers, riser systems, and offshore platforms. These complex structures usually have bluff cylindrical shapes which are conducive to vortex shedding when they are placed in a flow. In air, chimney stacks, high-tension power lines and bus bars commonly vibrate due to vortex shedding.

Reliable experimental data are now reasonably well in hand for dynamic response characteristics and flow-induced forces on a model scale. Based upon these experiments, semi-empirical prediction models have been developed and have been compared favorably with field test data.

BASIC CHARACTER OF VORTEX SHEDDING

The frequency f_s of the vortex shedding from a circular cylindrical member such as a cable or a riser is related to the other main flow parameters (D, the diameter; V, the flow velocity) through the nondimensional Strouhal number which is defined as

$$St = \frac{f_s D}{V}.$$

The value of the Strouhal number varies somewhat in different regimes of the Reynolds number and with the shape of the cylinder (circular, D-section, triangular, etc). For the range of the Reynolds number where the Strouhal number remains constant the relation between the shedding frequency and the velocity is linear for a given cylinder, i.e.

$$f_s = KV,$$

where $K = St/D$. If a cylinder immersed in a flowing fluid is free to oscillate in the cross-flow direction, then the latter relation does not hold in the vicinity of the natural frequency of the cylinder. This resonance phenomenon—called "lock-on" or "wake capture"—is discussed in this paper.

If the Reynolds number is lower than about 10^5, then the vortex shedding is predominately periodic and the value of the Strouhal number can be assumed to be about $St = 0.2$ for a circular cylinder or cable. Measurements of the frequencies, displacement amplitudes and forces which result from vortex-excited oscillations have been obtained by many investigators from experiments both in air and in water. The basic aspects of the problem of vortex-excited oscillations in general have been reviewed recently by Sarpkaya (1) and Bearman (2). King

(3), and Griffin and Ramberg (4) have discussed the subject in the context of marine applications.

AMPLITUDES OF DISPLACEMENT

It has been shown by numerous investigators (see references 2 and 3, for example) that the displacement amplitude is a function primarily of a response or "reduced damping" parameter of the overall form

$$k_s = \frac{2m\delta}{\rho D^2}. \tag{1}$$

This formulation of the reduced damping also is often written in the analogous form

$$\zeta_s/\mu = 2\pi\, St^2 k_s \tag{2}$$

when the damping is small and $\zeta_s = \delta/2\pi$. The importance of the reduced damping follows directly from resonant force and energy balances on the vibrating structure. It is important to note that the damping coefficients ζ_s and δ represent the damping measured in *still air*. For all practical purposes this is then equivalent to in vacuo structural damping. Moreover, the relation between Y_{MAX} and k_s or ζ_s/μ holds equally well for flexible cylindrical members with normal mode shapes given by $\psi_i(z)$, for the i th mode.

If the cross flow displacement (from equilibrium) of a flexible structure with normal modes $\psi_i(z)$ is written as

$$y_i = Y\psi_i(z) \sin \omega t \tag{3}$$

at each spanwise location z, then the peak displacement can be scaled by the factor

$$Y_{EFF,MAX} = Y\Gamma_i^{1/2}/|\psi_i(z)|_{MAX} = Y/\gamma_i, \quad Y = \bar{Y}/D, \tag{4a}$$

where

$$\Gamma_i = \frac{\int_0^L \psi_i^4(z)\, dz}{\int_0^L \psi_i^2(z)\, dz}, \tag{4b}$$

and

$$\gamma_i = \frac{|\psi_i(z)|_{MAX}}{\Gamma_i^{1/2}} \tag{4c}$$

The effective displacement amplitude Y_{EFF} is derived from considerations based on several versions of the so-called "wake oscillator" formulation for modelling vortex-excited oscillations (5,6).

Experimental data for Y_{EFF} as a function of ζ_s/μ are plotted in Fig. 1. These results encompass a wide range of single cylinders of various configurations and flexure conditions at Reynolds numbers from 300 to 10^6. For *all* of the data points plotted in Fig. 2 the damping coefficients ζ_s and/or δ were measured in *still* air. This should minimize any further misconceptions among other investigators who have discussed various versions of this figure. The various types of structures represented by the data points available through 1982 are given by Griffin and Ramberg (4). As a typical example, the deflections of a flexible cantilever in the fundamental mode have been measured under a variety of conditions. Peak-to-peak displacements as great as two to four diameters in water were measured for length/diameter ratios up to about $L/D = 250$. All available experiments conducted to date indicate that the limiting unsteady displacement amplitude for a flexible circular cylinder is about $Y_{EFF} = \pm 1$ at the lowest values of reduced damping.

The most recent measurements in water shown in Fig. 1 have been provided by Every and King (7) and by Moe (8) and are given by the symbols ❶ and ❷ respectively. Both provide additional confirmation of the earlier trends shown in the figure. It is interesting to note that the reduced damping can increase from $\zeta_s/\mu = 0.01$ to 0.5 (a factor of *fifty*) and the displacement amplitude decreases only from two or three diameters to one diameter (a nominal factor of only *two or three*). This is why it is difficult to suppress the in-water oscillations by means of mass and damping control. Recent discussions of the suppression of vortex-excited oscillations in water are given by Every, King and Griffin (7,9) and by Zdravkovich (10).

The situation is somewhat different in air as shown in Fig. 2, which has been adapted from Adami and Batch (11). The vibrations of a slender model ($L/D = 114$) were measured in a wind tunnel with different end fixities. For the conditions tested the vibrations were nearly independent of the mode, end conditions and the aspect ratio (11). The solid line drawn in the figure is the prediction

$$\bar{Y}_{MAX}/D = \frac{1.29\ \gamma_i}{[1 + 0.43\ (4\pi\ St^2 m\delta/\rho D^2)]^{3.35}} \qquad (5)$$

This is a least-squares fit to the data in Fig. 2 which were available in 1977. Other virtually identical prediction curves derived by different methods have been proposed by Sarpkaya (1), Iwan (6) and Blevins (12). The data plotted in Fig. 2 are typical of those obtained in air and would fall toward the right-hand side of Fig. 1. In that region the displacement amplitude is strongly dependent on the reduced damping. Control of the mass and damping of the member then provides a means for suppressing the vibrations.

These results have been obtained both in air and in water, even though the mass ratios of vibrating structures in the two media differ by two orders of magnitude. For typical structures vibrating in water the mass ratio $\frac{m}{\rho D^2}$ varies from slightly greater than 1 to about 5; in air the mass ratios corresponding to Figs. 1 and 2 typically vary from $\frac{m}{\rho D^2} = 15$ to 500.

LIFT FORCES

The resultant unsteady fluid force which acts on a resonantly vibrating, cylindrical structure due to vortex shedding can be divided into several components (13), which are:

- An exciting component of the lift force, by which energy is transferred to the structure;
- A reaction, or damping force, which is exactly out-of-phase with the structure's velocity;
- An "added mass" force, which is exactly out-of-phase with the structure's acceleration; and
- A flow-induced inertial force.

These various contributions to the total force can be deduced from the total hydrodynamic force as reported, say, by Sarpkaya (1) or the various components can be measured individually (see reference 13). The present brief discussion will deal essentially with the exciting force which drives the vibration.

The exciting force coefficient force is defined as

$$C_{LE} = C_L \sin\phi \qquad (6)$$

and is important because it is the component of the total force that transfers energy to the vibrating structure. Here ϕ is the phase angle between the hydrodynamic force coefficient C_L and the displacement of the structure. A relatively large number of measurements of C_{LE} by

various means are plotted against the effective displacement amplitude Y_{EFF} in Fig. 3. Table 1 describes the various conditions under which the experimental results were obtained. There is some scatter in the various measured values of C_{LE}, but certain trends are clear. First there is a maximum of the excitation force coefficient at a peak-to-peak displacement amplitude of between 0.6 and 1 diameters for all the cases shown in the figure. Second, the maximum of the force coefficient is approximately $C_{LE} = 0.5$ to 0.6 for all but one case; the single exception is the result at $C_{LE} = 0.75$ measured by Sarpkaya. C_{LE} then decreases toward zero and results in a limiting effective displacement amplitude between two to three diameters. This limiting amplitude is clearly shown at the low values of reduced damping in Fig. 1.

DRAG FORCES

An important consequence of the resonant cross flow oscillations of structures and cables due to vortex shedding is an amplification of the steady drag force (or equivalently the drag force coefficient C_D). The drag amplification under a variety of conditions has been measured and the results have been summarized by Griffin and Ramberg (4). A step-by-step for employing these measurements in the analysis of marine cable structures was developed by Skop, Griffin and Ramberg (16). One step in the method uses Eq. (5) to predict the cross flow displacement amplitude of the member. Measurements of the drag coefficient more recent than those discussed by Griffin and Ramberg are presented here.

Measurements of the vortex-induced cross flow vibrations of model marine piles were made by Fischer, Jones and King (17,18). The steady deflection at the free end of the model pile also was measured; in this case the model was a simple, uniform cantilever beam with no tip masses, fully immersed in water, and normal to the incident flow. For low flow velocities the measured and predicted tip deflections coincided when the pile was effectively stationary. The deflection was predicted by assuming a uniform loading

$$w(x) = 1/2\,\rho V^2 D C_D(x) \tag{7}$$

over the length of the flexible beam in which the drag coefficient $C_D(x)$ was a constant, $C_D = 1.2$.

When the critical flow velocity for the onset of the vortex-induced vibrations was exceeded, the measured steady deflections in line with the flow departed significantly from the

Table 1
The Excitation Force Coefficients on Vibrating Bluff Cylinders; Description of the Data in Fig. 3

Symbol	Type of cylinder	Medium	Cylinder material	Investigator(s)
▲	Flexible cantilever	Water	PVC	King (1977)
■			PVC	
			Aluminum	
			Stainless steel	
○	Pivoted rigid cylinder	Water & Air	Brass	Vickery and Watkins (1964)
+	Spring-mounted rigid cylinder	Air	Aluminum tubing	Griffin and Koopmann (1977)
◑	Rigid cylinder, forced oscillations	Water	Aluminum tubing	Sarpkaya (1978)
Δ	Flexible cantilever	Air	Aluminum	Hartlen, Baines and Currie (1968)
●	Flexible cylinder	Air	—	Farquharson and McHugh (1956)†
◐	Rigid cylinder forced oscillations	Air	Brass	Simmons and Cleary (1979)

†Quoted by Simmons and Cleary.

Table 2
Drag Force Amplification on Vibrating Circular Cylinders; Description of the Data in Fig. 6

Symbol	Medium	Type of Vibration	Investigator(s)
⊕	Air	Cross flow, forced	Griffin and Ramberg (1975)
◇	Water	Cross flow, forced	Sarpkaya (1977)
□	Water	Cross flow, forced	Schargel (1980)
X	Water	Cross flow, free	Overvik (1982)
◓, ◒	Water	Cross flow, free	Moe (1982)

predicted reference curve. One example of the results obtained is given in Fig. 4. Flow velocities above the threshold value caused steady deflections of up to twice the model's value predicted by assuming $C_D = 1.2$. At the higher values of relative density of the model structure to the density of water, the steady deflections of the model diverged from the predicted curve, reached a maximum value as shown in Fig. 4, and then returned to the predicted curve obtained with $C_D = 1.2$. The pile tip was deflected in line about 1.3 diameters at a water velocity V of 0.6 kt (0.3 m/s) for the conditions of Fig. 4. At this same flow velocity the cross flow displacement amplitude was ± 1.5 diameters. If the pile was restrained from oscillating, then the steady in-line deflection of the tip was predicted to be 0.6 diameters at the same flow velocity. The predicted tip deflections for the oscillating pile in Fig. 4 were computed using a method described by Every, King and Griffin (9).

The mean vortex-induced drag coefficient C_D on a freely-oscillating, spring-mounted cylinder is plotted against the reduced velocity V_r in Fig. 5. The measurements were made by Overvik (19) as a baseline case in a more extensive study of the effects of vortex shedding on marine risers. The drag on the cylinder clearly undergoes a resonant-like behavior in much the same manner a the cross flow displacement amplitude. Comparable measurements by Overik of the displacement amplitude $\bar{Y}/D$ correspond directly with the behavior of the drag coefficient C_D. At the peak value of the response, $\bar{Y} = 1.1\ D$, the drag coefficient is $C_D = 2.5$. This is an amplification of about 250 percent, which is of sufficient magnitude to cause severe problems for the designer of marine structural members of cylindrical cross section. Less severe problems develop in the case of structures in air because of the smaller vibration amplitudes which are common there.

The drag amplification C_D/D_{D0}, where C_{D0} is the drag coefficient for the stationary cylinder, from a variety of recent experiments is plotted in Fig. 6 as a function of the "wake response" parameter

$$w_r = (1 + 2\ \bar{Y}/D)\ (V_r St)^{-1}. \tag{8}$$

This parameter was proposed by Skop, Griffin and Ramberg (16) as a means for correlating the drag amplification that accompanies vortex-induced vibrations. In the particular form shown the factor St^{-1} acts to correct for any variations in Strouhal number (and Reynolds number) among the various sets of data. All of the data in Fig. 6 refer to conditions of lock-in between

the vortex and vibration frequencies. A previous drag amplification-wake response parameter plot (16) for the deflection predictions shown in Fig. 4.

It is interesting to note the variety of data which are correlated in the figure. For instance, the drag coefficients from Griffin and Ramberg (20) were derived from wake measurements with a forced-vibrating cylinder in air. The drag measurements from Sarpkaya (21) and Schargel (22) were made on a forced-vibrating cylinder in water. Moe (8) and Overvik (19) measured the drag on a freely-vibrating cylinder in water. All of these different experiments resulted in substantial amplifications of the drag coefficient, with $C_D/C_{D0} > 2$ not uncommon for both free and forced vibrations in water.

Similar levels of hydrodynamic drag amplification were measured during the recent field experiments reported by Vandiver and Griffin (23,24). Both a 23 m (75 ft) long pipe and a cable with and without attached masses underwent large-amplitude vibrations ($\bar{Y} = \pm\ 1D$) due to vortex shedding in a steady current. Mean drag coefficients of $C_D = 2.4$ to 3.2 were measured during the time intervals when the pipe and cable were strumming at these large amplitudes. In another recent series of experiments Davies and Daniel (25) measured the strumming vibrations of submersible umbilical cables. The model cable of L/D = 100 to 300, which was tested in a large water channel, consistently was excited into large-amplitude cross flow oscillations which were comparable in level to those reported by Vandiver and Griffin. Consequently the normal mean drag coefficients measured by Davies and Daniel were in the range $C_D = 2.5$ to 3.4. This is an amplification factor of 2 to 2.8.

The overall implications for practical applications are that the relatively large amplitudes of vibration caused by vortex shedding, and the amplifications of the unsteady and steady fluid forces which are a consequence of the vibrations, can cause both large steady deflections and stresses and time dependent, fatigue-related unsteady forces and stresses.

SUMMARY AND CONCLUDING REMARKS

Until recent years problems associated with vortex shedding in marine applications were investigated on an ad hoc case-by-case basis, largely because reliable experimental data and design procedures were not available for general use. However, the dynamic analysis of structures and cable systems has become increasingly important and sophisticated because the

amplitudes of vibration for a cylindrical structure such as a riser or pipeline in water are an order of magnitude greater than for a similar structure in air. The small mass ratio (structure to displaced fluid) in water produces in turn small values of the reduced damping which then contribute to the relatively large vibration amplitudes shown here in Fig. 1.

There is a large range of reduced damping over which bluff cylindrical structures in water undergo large-amplitude vibrations ($\bar{Y} > \pm 1D$) due to vortex shedding. Thus it is not possible to suppress these oscillations by means of mass and damping control, and some form of external device such as a helical strake winding or fairing is required. The unsteady component of the lift coefficient which drives the vibration is increased, as is the mean in-line drag coefficient which is increased by as much as 250 percent.

Structures in air experience vibration amplitude levels much smaller in magnitude, and consequently the drag amplification is not as extreme as in water. Mass and damping control often is used to suppress the in-air vibrations of cables and slender pipes; external devices such as helical strakes also are used on stacks and the protruding legs of jack-up drilling rigs under tow.

ACKNOWLEDGMENT

This paper was prepared at the Naval Research Laboratory as part of a research program supported by the Minerals Management Service of the U.S. Department of the Interior.

REFERENCES

1. T. Sarpkaya, "Vortex-Induced Oscillations, A Selective Review," Trans. ASME, J. Applied Mechanics, Vol. 46, 241-258, 1979.

2. P. W. Bearman, "Vortex Shedding From Oscillating Bluff Bodies", Ann. Rev. Fluid Mech., Vol. 16, 195-222, 1984

3. R. King, "A Review of Vortex Shedding Research and Its Applications," Ocean Engineering, Vol. 4, 141-171, 1977.

4. O.M. Griffin and S.E. Ramberg, "Some Recent Studies of Vortex Shedding with Application to Marine Tubulars and Risers," Trans. ASME, J. Energy Resources Tech., Vol. 104, 2-13, 1982.

5. R.A. Skop and O.M. Griffin, "On a Theory for the Vortex-Excited Oscillations of Flexible Cylindrical Structures," J. Sound and Vib., Vol. 41, 263-274, 1975; see also "The Vortex-Induced Oscillations of Structures," J. Sound and Vib., Vol. 44, 303-305, 1976.

6. W.D. Iwan, "The Vortex-Induced Oscillation of Elastic Structural Elements," Trans. ASME, Series B, J. Engrg. Indus., Vol. 97, 1378-1382, 1975.

7. M.J. Every and R. King, "Suppressing Flow-Induced Vibrations—An Experimental Study of Clamp-On Devices," BHRA Fluid Engineering Report RR 1576, November 1979.

8. G. Moe, Private communication, 1983.

9. M.J. Every, R. King and O.M. Griffin, "Hydrodynamic Loads on Flexible Marine Structures due to Vortex Shedding," Trans. ASME, J. Energy Resources Tech., Vol. 104, 330-336, 1982.

10. M.M. Zdravkovich, "Review and Classification of Various Aerodynamic and Hydrodynamic Means for Suppressing Vortex Shedding," J. Indus. Aero. and Wind Engrg., Vol. 7, 145-189, 1981.

11. H. Adami and B.A. Batch, "Aeolian Vibrations of Tubular Busbars in Outdoor Substations," Electra, No. 75, 99-120, March 1981.

12. R.D. Blevins, *Flow-Induced Vibrations*, Van Nostrand Reinhold: New York, 1977.

13. O.M. Griffin, "Vortex-Excited Cross Flow Vibrations of a Single Cylindrical Tube," Trans. ASME, J. Press. Vessel Tech., Vol. 102, 158-166, 1980.

14. J.M. Simmons and P.M.G. Cleary, "Measurement of Aerodynamic Power Associated with Vortex-Induced Vibration of Electrical Transmission Lines," IEEE Power Engineering Society Paper F79 713-9, 1979.

15. F.B. Farquharson and R.E. McHugh Jr., "Wind tunnel investigation of conductor vibration with use of rigid models," Trans. AIEE, Vol. 75, 871-878, 1956.

16. R.A. Skop, O.M. Griffin and S.E. Ramberg, "Strumming Predictions for the SEACON II Experimental Mooring," Offshore Technology Conference Paper OTC 2884, May 1977.

17. F.J. Fischer, W.T. Jones and R. King, "Current-Induced Oscillations of Cognac Piles During Installation," in *Practical Experiences with Flow-Induced Vibrations*, E. Naudascher and D. Rockwell (eds.), Springer-Verlag: Berlin, 570-581, 1980.

18. R. King, "Model Tests of Vortex-Induced Motion of Cable Suspended and Cantilevered Piles for the Cognac Platform," BHRA Fluid Engineering Report RR 1453, January 1978.

19. T. Overvik, "Hydroelastic Motion of Multiple Risers in a Steady Current," Ph.D. Thesis, Norwegian Institute of Technology, August 1982.

20. O.M. Griffin and S.E. Ramberg, "On vortex strength and drag in bluff body wakes," J. Fluid Mech., Vol. 69, 721-728, 1975.

21. T. Sarpkaya, "Transverse Oscillation of a Circular Cylinder in Uniform Flow," Proc. ASCE, J. WPCO Div., Vol. 104, 275-290, 1978.

22. R.S. Schargel, "The Drag Coefficient for a Randomly Oscillating Cylinder in a Uniform Flow," M.S. Thesis, MIT Ocean Engineering Department, September 1980.

23. J.K. Vandiver, "Drag Coefficients of Long, Flexible Cylinders," Offshore Technology Conference Paper OTC 4490, May 1983.

24. O.M. Griffin and J.K. Vandiver, "Flow-Induced Vibrations of Taut Cables with Attached Masses," Naval Civil Engineering Laboratory Report CR 84.004, November 1983.

25. M.E. Davies and A. P. Daniel, "The Hydrodynamics of a Model of a Vibrating Umbilical Cable," Offshore Technology Conference Paper OTC 4832, May 1984.

Appendix I. NOTATION

The following symbols are used in this paper:

a_1, b_1, c_1, d_1	Coefficients in the lift coefficient C_{LF}, equation (16).
C_D, C_{D0}	Steady drag coefficient on a vibrating (stationary) cylinder or cable.
C_L	Lift coefficient; see equation (6).
C_{LF}	Excitation force coefficient; see equation (6).
D	Body diameter (m or ft).
f_n	Natural frequency (Hz).
f_s	Strouhal frequency (Hz).
I_i	Modal scaling factor; see equation (4).
k_s	Reduced damping; see equation (1).
L	Body length (m or ft).
m	Physical mass per unit length (kg/m or lb_m/ft).
m'	Virtual mass (physical plus added mass) per unit length (kg/m or lb_m/ft).
St	Strouhal number, $f_s D/V$.
V	Incident flow velocity (m/s or ft/sec or knots).
V_r	Reduced velocity, $V/f_n D$.
w_r	Response parameter, $(1 + 2\,\overline{Y}/D)\,(V_r \mathrm{St})^{-1}$; see equation (8).
$\overline{y}$, $\overline{Y}$	Cross flow displacement, displacement amplitude (m or ft).
Y	Normalized displacement amplitude, $\overline{Y}/D$.
$Y_{EFF,MAX}$	Normalized displacement amplitude; see equation (4).
z	Coordinate measurement along the cylinder or cable (m or ft).
δ	Log decrement of structural damping; see equation (1).
γ_i	Normalizing factor; see equation (4).
ϕ	Phase angle (deg. or rad); see equation (6).
μ	Mass ratio, see equation (2).
ν	Kinematic fluid viscosity (m^2/sec or ft^2/sec).
ρ	Fluid density (kg/m^3 or lb_m/ft^3).
$\phi_i(z)$	Mode shape for ith flexible beam mode; see equation.
ζ_s	Structural damping ratio; see equation (2).

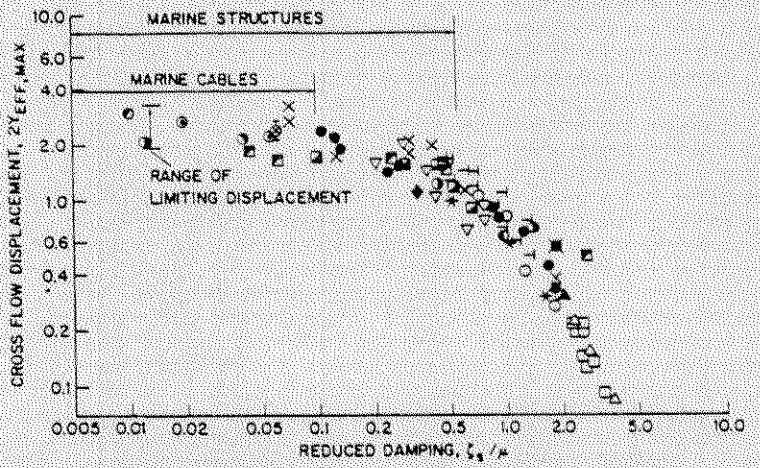

Fig. 1 — The maximum cross flow displacement amplitude, $2Y_{EFF,MAX}$, of circular cylindrical members, scaled as in Eq. (4), as a function of the reduced damping, $k_s = 2\pi S^2 \delta$. The legend for the data points is given in Ref. (4), except for the recent data of Moe (1982), Q and of Every and King (1974), B.

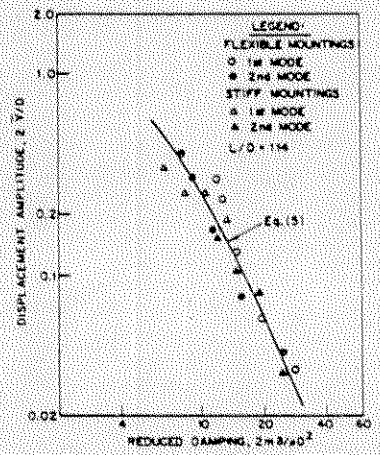

Fig. 2 — The cross flow displacement amplitude, $2\overline{Y}/D$, for flexible circular cylinders in a wind tunnel as a function of the reduced damping, $k_s = 2m\delta/\rho D^2$; adapted from Adams and Basch (1981).

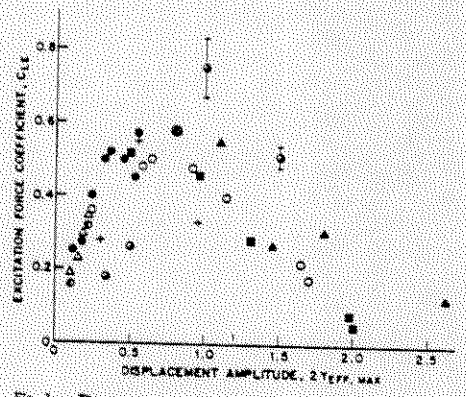

Fig. 3 — The component, C_{LE}, of the lift force plotted against the displacement amplitude $2Y_{EFF\ MAX}$, scaled as in Eq. (4). The legend for the data points is given in Table 1.

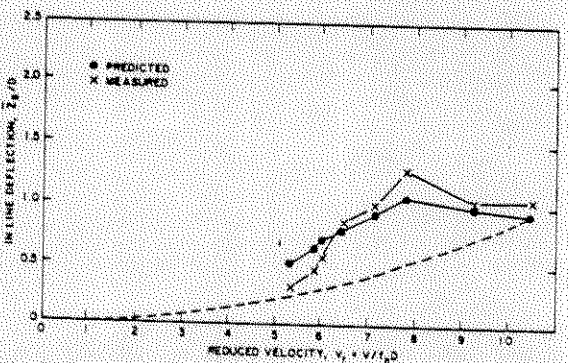

Fig. 4 — The predicted and measured steady tip deflection, $\bar{Z}_g/D$, for a vibrating flexible cantilever in water; from Every, King and Griffin (1982). Relative density of the beam, SG = 3.5; — — — —, beam restrained from oscillating, $C_{De} = 1.2$.

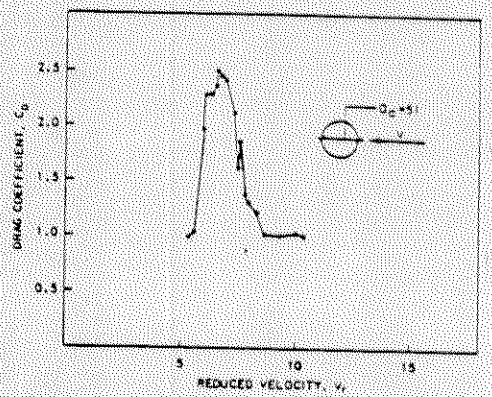

Fig. 5 — The drag coefficient, C_D, plotted against the reduced velocity, V_r, for a spring-mounted circular cylinder; from Every, King and Weaver (1982). Peak cross flow displacement amplitude, $\hat{Y} = \pm 1$ to $1.1D$.

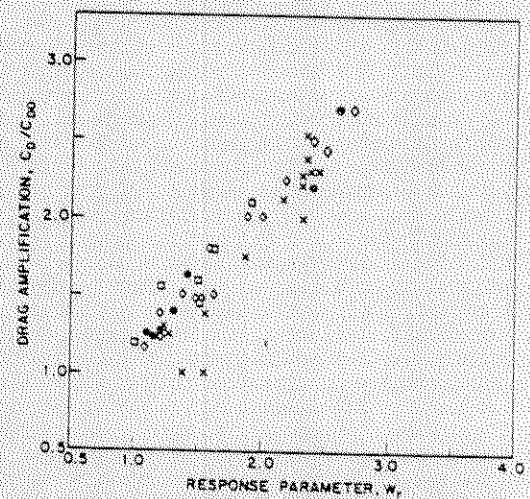

Fig. 6 — The drag coefficient amplification, C_D/C_{De}, plotted as a function of the wake response parameter, $W_r = (1 + 2\hat{Y}/D)\ (St\ V_r)^{-1}$, for the cross flow vibrations of a circular cylinder. The legend for the data points is given in Table 2.